# Characterization of Starburst Dendrimers and Vesicle Solutions and Their Interactions by CW- and Pulsed-EPR, TEM, and Dynamic Light Scattering

**M. Francesca Ottaviani* and Paolo Matteini**

*Department of Chemistry, University of Florence, Via G. Capponi 9, 50121 Firenze, Italy*

**Marina Brustolon**

*Department of Physical Chemistry, University of Padua, Via Loredan 2, 35131 Padova, Italy*

**Nicholas J. Turro and Steffen Jockusch**

*Department of Chemistry, Columbia University, New York, New York 10027*

**Donald A. Tomalia**

*Michigan Molecular Institute, Midland, Michigan 48640*

*Received: January 8, 1998; In Final Form: May 8, 1998*

Starburst dendrimers (SBDs) of different generations (size) and level of protonations of their surface amino groups and solutions of dimyristoylphosphatidylcholine (DMPC) vesicles were analyzed, both separately and in mixtures of the two components, by negative-staining transmission electron microscopy (TEM), dynamic light scattering (DLS), and, mainly, by computer-aided continuous wave (CW)- and pulsed-electron paramagnetic resonance (EPR). For the EPR study, the SBDs were labeled with a nitroxide radical (SBD-T). TE micrographs showed the vesicles as multilamellar structures of spherical shape with diameters ranging from 0.2 to 1.2 m. DLS measurements provided the mean vesicle diameter ($d$) at ca. 400 nm, whereas the diameter of generation 6 was 7 nm. No large-sized permanent supramolecular structures ($d$ > 400 nm) were formed. EPR measurements at room temperature were poorly informative, since (1) a fraction of the dendrimers was not interacting with the vesicles, and (b) the labels that were interacting with the vesicles were rotating quickly around the main axis. Interactions between the dendrimers and the vesicles (tested by a decrease in rotational mobility of the label) became EPR-observable and quantifiable below the freezing transition of a portion of the solution, which could not be detected by EPR analysis. The fraction of the dendrimers interacting with the vesicles underwent a glass transition. Dendrimer−vesicle interactions modified the direction of the fast-rotation axis of the radical, and the interaction was more effective for protonated dendrimers of a larger size, i.e., later generation. A "complex" was formed between one solvent molecule and the nitroxide radical. Interactions between the SBD-T and the vesicle partially compressed the hydration layer of the N−O group, and/or the hydration layer of the vesicle headgroups was compressed onto the unpaired-electron site. This study provides information on the possible utilization of starburst dendrimers as gene carriers.

## Introduction

Curved bilayers and multilayers, termed vesicles and liposomes,[1,2] are widely employed as models of biological membranes.[3−5] In this study, we explore interactions between liposomes formed by dimyristoylphosphatidylcoline (DMPC) and dendritic macromolecules[6,7] termed starburst dendrimers.[7] These highly ordered hyperbranched arrays are composed of amidoamine units emanating from a central ethylenediamine core and terminating in amino groups. Subsequent concentric layers are termed generations: three to four generations (earlier generations) form an open structure; beyond four generations (later generations) there is formed a densely packed external topology.[8] These dendrimers will be henceforth termed *n*SBD (where *n* indicates the generation).

The supramolecular dendrimer−liposome assembly, such as a host−guest system, holds great interest for the general fields of membrane transport and drug delvery.[9] Water-soluble polymers have been proposed as drug delivery agents.[10] A general strategy is to design polymers capable of (i) temporarily inactivating a drug, typically by a supramolecular encapsulation through adsorption, (ii) carrying the encapsulated drug to a target cell, and (iii) assisting in the passage of the drug through the cell membrane and into the cell.

We have used dynamic light scattering (DLS) and negative-staining transmission electron microscopy (TEM) for a preliminary characterization of the DMPC-liposomes and the *n*SBDs in a water solution and in liposome−dendrimer mixtures. Light scattering techniques have demonstrated to be a powerful tool in characterizing vesicles, in particular phosphatidylcholine vesicles.[13] On the other hand, negative-staining TEM has already been shown by other authors to provide information on the size and morphology of vesicles in solution.[14,15]

Additionally, EPR techniques have been extensively used to study vesicles and liposomes and molecules interacting with

* To whom correspondence should be addressed.

S1089-5647(98)00715-9 CCC: $15.00 
Published on Web 07/15/1998

**SCHEME 1**

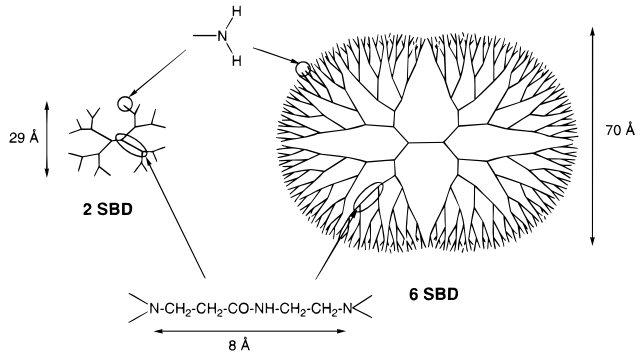


them.[16−19] Recently, the EPR technique has been applied to characterize *n*SBD solutions both in the absence and in the presence of surfactants and surfactant aggregates.[20−22] Surfactant aggregates also mimic the simplest membrane model. Formation of supramolecular dendrimer−surfactant structures has been described as being comparable to nSBDs with biomimetic ordered assemblies.[21,22] In addition to structural information, mobility and polarity parameters may be extracted from analysis of the continuous-wave (CW) EPR spectra of spin probes or spin labels,[23] whereas analysis of the electron spin−echo (ESE) spectra provides information on the structure of the radical environment.[24] Electron spin−echo envelope modulation (ESEEM) studies of phospholipid vesicles with embedded probes have already been shown to provide interesting information about the vesicle structure.[25] Furthermore, ESEEM studies have been carried out to describe the interactions of *n*SBDs with SDS micelles.[26] The structure of the micelle changes upon interaction with the dendrimers, allowing water permeability at the radical site.

Against this background we have performed a computer-aided analysis of the CW-EPR and ESEEM spectra of the DMPC-vesicle−*n*SBD system. Since interest was directed to dendrimer−liposome interactions, we decided to use dendrimers spin-labeled with a nitroxide radical (2,2,6,6 tetramethylpiperidine-*N*-oxyl, termed Tempo). The Tempo radical, by following the fate of the *n*SBDs, directly monitored the localization of the dendrimers in the vicinity of the liposome surface as well as modifications of the interface properties due to dendrimer−liposome interactions. For this reason we selected 2SBD and 6SBD as representatives of earlier and later generations, respectively. Scheme 1 shows a bidimensional view of these SBDs. Finally, *n*SBD−vesicle interactions were investigated as a function of the level of protonation of the amino groups at the *n*SBD surface.

## Experimental Section

Water solutions were prepared using doubly distilled water filtered through Millipore filters.

DMPC was purchased from Sigma and used as received. The liposomes were obtained following the procedure described by Reeves and Dowben.[27] After drying down the lipid film, hydration was initiated by exposing the film to a stream of water-saturated nitrogen followed by swelling in a sucrose solution without shaking. Spinning allowed for the removal of floating multilamellar vesicles. Addition of a glucose solution and further spinning produced a pellet of vesicles. The maximum concentration of the vesicles in the solutions employed in the present study was in the range $10^{-9}$−$10^{-10}$ M.

The SBDs employed in this study were synthesized as described in previous papers.[7] Accurate purification of the dendrimers was accomplished from subsequent recrystallization in water solutions. Their purity was carefully controlled by mass spectrometry.[28]

The labeling of the dendrimers (*n*SBD-T) was accomplished employing a modified method used by G. T. Pauly et al. for labeling of DNA.[29] To a solution of 0.2 mmol (in surface groups) of *n*SBD in 4 mL of 0.1 M $Na_3BO_3$ (Aldrich) was added 0.02 mmol 4-(2-iodoacetamido)-Tempo (Aldrich) in 0.1 mL DMF and stirred for 6 h at room temperature. The mixture was then extracted four times with methylene chloride and hexane to remove free Tempo. For further purification, dialysis in water was used, employing a Spectra/Por cellulose ester membrane (MWCO:2000) (Spectrum Medical Industries, Inc.). The labeling grade was evaluated as 1 label for about 30 surface amino groups.

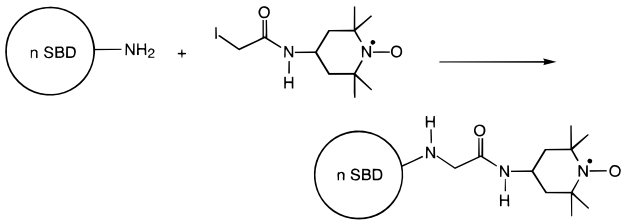


Water solutions of 2SBD-T and 6SBD-T were prepared at a concentration of 0.1 M in surface amino groups. Unless otherwise specified, the concentration of the SBD solutions is in the surface groups. The solutions were stored under nitrogen to avoid oxidation degradation and kept under refrigeration until used. Protonation of the surface amino groups was accomplished by adding controlled amounts of diluted HCl (0.05 M, Merck). The acid−base properties of the SBDs have already been determined in a previous study.[30] The protonated SBD-T will henceforth be termed *n*SBD-$T^+$.

The dendrimer solutions were then added to the DMPC-liposome solutions to obtain a final concentration of 0.05 M in surface amino groups.

The EPR spectra were recorded using a Bruker 200D spectrometer operating at X band (9.5 GHz), interfaced with Stelar software to a IBM PC computer for data acquisition and handling. The temperature was controlled with the aid of a Bruker ST 100/700 variable-temperature assembly.

The preparation procedure to provide the samples for the ESE measurements was as described above for obtaining the DMPC vesicles, the labeled dendrimers, and the dendrimer−vesicle solutions, but $D_2O$ (Merck, purity 99.8%) was used instead of $H_2O$. All procedures were carried out under a nitrogen atmosphere. Deuterated water was used to distinguish modulation due to the deuterium nuclei of the solvent from the modulation due to protons belonging to the dendrimer or the liposome surface.

Quartz EPR tubes were used for the ESE measurements.

The ESE experiments were carried out at 4 K with the aid of a Bruker ESP 380E FT-EPR spectrometer equipped with a liquid helium cooling accessory ER4112HV. On the basis of previous literature we assumed that the structure of the dendrimers and the liposomes and of the supramolecular arrangements, *n*SBD-T−DMPC, were retained at 4 K, under the conditions of rapid freezing of the solutions.[25b,31]

Two-pulse (2p) spin−echo signals were registered by varying $\tau$, the time between pulses. The pulse sequence was (16-$\tau$-32 ns). Three-pulse (3p) echoes were registered by varying $T$, the time between the second and the third pulses. The pulse sequence was (16-$\tau$-16-$T$-16 ns). Six modulated echo decays

were collected at $\tau = 160$, 168, 176, 184, 192, and 200 ns. The magnetic field was set at 3483 G, corresponding to the central line. However, settings on the lateral lines produced the same ESE signal.

Transmission electron microscopy (TEM) measurements were performed within 1 day of preparation applying the negative-staining technique.[32] The samples were stained with 2 wt %/wt uranyl acetate for 2 h after adsorption onto a nickel net, covered by Formvar (poly(vinyl formaldehyde)) film. TEM measurements were obtained by means of PHILIPS-EM 201-TEM instrumentation.

Dynamically scattered light measurements were performed on diluted (1:10) solutions upon double filtration by means of a 650 nm pore filter. DLS was measured at 25 °C on a Spectra Physics 2030 light scattering spectrophotometer at 514.5 nm wavelength of an argon laser. The spectrophotometer was equipped with a BI-200 goniometer and a BI-2030 correlator (Brookhaven). The DLS facilities were kindly provided by Ausimont-Bollate (Milan, Italy).

Reliability of the results reported and discussed in the Results and Discussion section was tested by the reproducibility of the results themselves for several preparations of samples and repeated experimental measurements.

## Theoretical Section

**(1) Analysis of the CW-EPR Spectra.** Computer-aided analysis of the EPR spectra, by means of the well-established procedure developed by Schneider and Freed,[33] provides the following parameters. (a) One parameter is the correlation time for rotational motion of the nitroxide group, assuming a Brownian model for rotational mobility. The main axis of rotation may change: the *Z* axis corresponds to the direction of the p orbital containing the unpaired electron, whereas the *X* axis lies in the N−O bond direction. A further tilting of the main rotation axis with respect to the magnetic axis is also included in the calculation. An averaged $\langle\tau\rangle$ is obtained, i.e., $\langle\tau\rangle = (\tau_{\parallel}\tau_{\perp})^{1/2}$ (the accuracy of $\langle\tau\rangle$, as obtained from spectral computation, is 2%). A decrease in mobility, i.e., an increase in $\langle\tau\rangle$, is indicative of the localization of the probe in more viscous environments, such as the liposome/dendrimer interface. (b) The second parameter is the set of principal components of the **g** tensor (assuming that the Zeeman coupling between the electron spin and the magnetic field is constant): $g_{xx} = 2.009$, $g_{yy} = 2.006$, $g_{zz} = 2.003$; the hyperfine **A** tensor components (for the coupling between the unpaired electron spin and the nuclear nitrogen spin) of SBD-T in water solution were found to be $A_{xx}$= 6 G, $A_{yy} = 8$ G, and $A_{zz} = 39$ G. The variation of $A_{zz}$ is assumed to be a measure of the environmental polarity and/or of the probe mobility: a decrease in $A_{zz}$ reflects a decrease in the polarity of the radical environment or an increase in mobility (accuracy of $A_{zz}$, as obtained from spectral computation, is 2%). (c) The third parameter is the partition of the probes in different environments, assuming the exchange is slow on the EPR time scale. This gives rise to the superposition of different signals that constitute the overall EPR line shape. A subtraction procedure of the computed components from the experimental signal, together with an addition procedure of the computed components to reproduce the experimental signal, allowed the extraction of each component and the different percentages of the components. Precision in the parameters decreased for more than two components.

**(2) Analysis of the ESE Spectra.** Both the two pulse ($\pi$/2-$\tau$-$\pi$) Hahn echo and the three-pulse ($\pi$/2-$\tau$-$\pi$/2-*T*-$\pi$/2) stimulated echo were recorded and analyzed.

In the two-pulse experiment, the echo intensity is monitored by varying the time interval $\tau$ between the two pulses. The exponential decay time is the so-called phase memory time $T_M$, which has been shown to be determined for nitroxide radicals at low temperature by the secular and pseudosecular processes due to modulation of the hyperfine coupling constants of the rotating methyl protons.[34] Therefore, $T_M$ gives directly the correlation time of the methyl group rotation, $\tau_c$. Moreover, the decay trace can be modulated by nuclear frequencies. For an electron coupled by dipolar interaction with a nucleus, the Hahn echo decay will be modulated by the two ENDOR frequencies $\nu_4$ and $\nu_-$, their sum and their difference.[35,36]

In the case of the three-pulse experiment, the decay of the echo is observed upon varying the time interval *T* between the second and the third pulses. The exponential decay time is the longitudinal relaxation time, $T_1$, which is longer than the transverse relaxation time in the solid state.[37] In particular, for values of $\nu$ and $\tau$ such that $\nu_{\pm}\,\tau = n$, where n is an integer, the modulation at the corresponding frequency disappears.[38] To avoid the latter "blind spots", we have collected a series of six echo decays varying $\tau$ between 160 and 200 ns.

The modulated decay curve in both experiments can be described by a function[39] $V(t) = V_m(t)\,V_d(t)$, where $V_m(t)$ describes the modulation pattern, and $V_d(t)$ the decay function. The procedure of simulation of the ESE spectra has been described by Romanelli and Kevan.[40] Analysis of the modulation pattern is based on the assumption of isotropic shells of weakly coupled nuclei around the electron spin distribution at distances below 0.6 nm. The simulation is done with a best fit procedure in which the parameters are the type and number $n^0_i$ of nuclei inducing modulation, their distance from the paramagnetic center $r_i$ (accuracy of $r_i$, as obtained from computation, is ±0.005 nm), and their hyperfine coupling constants $a_i$ (accuracy of $a_i$, as obtained from computation, is ±0.02 MHz). In the case of deuterium, the modulation function $V_m(t)$ was computed by means of the second-order perturbation approach derived by Heming et al.[41]

The modulation pattern is not affected by the protons of the methyl groups attached to the piperidine ring. In fact, the modulation depth in ESEEM spectra for each coupled nucleus depends on the anisotropy of the corresponding hyperfine tensor,[42] which, for the methyl groups, is averaged by rotation. In fact, it has been reported that the methyl group rotation of methyl-substituted benzenes is quite fast ($3 \times 10^{-5}$ s) even at 4 K.[43]

Calculation of the decay pattern provides the correlation time $\tau_c$ for the rotation of the methyl groups (accuracy of $\tau_c$, as obtained from calculation, is 10%).

**(3) Analysis of Light Scattering Results.** Multiangle dynamic light scattering measures the time variation of the intensity and the phase of the light which diffuses at fixed angles. DLS has been profitably utilized for determining the particle size distribution.[44,45] The shape of the autocorrelation functions at each diffusion angle depends on the amount of scattering of each component at different sizes. The salient points of the theoretical analysis are described in the following paragraph.[45,46]

The experiment measures the normalized intensity (photon count) autocorrelation function of the scattered light:

$$g^{(2)}(\tau) = 1 + B|g^{(1)}(\tau)|^2$$

The instrumental constant *B* is scaled out during the analysis and, therefore, has no influence on the results. $g^{(1)}(\tau)$ is the electric field autocorrelation function. For a monodisperse

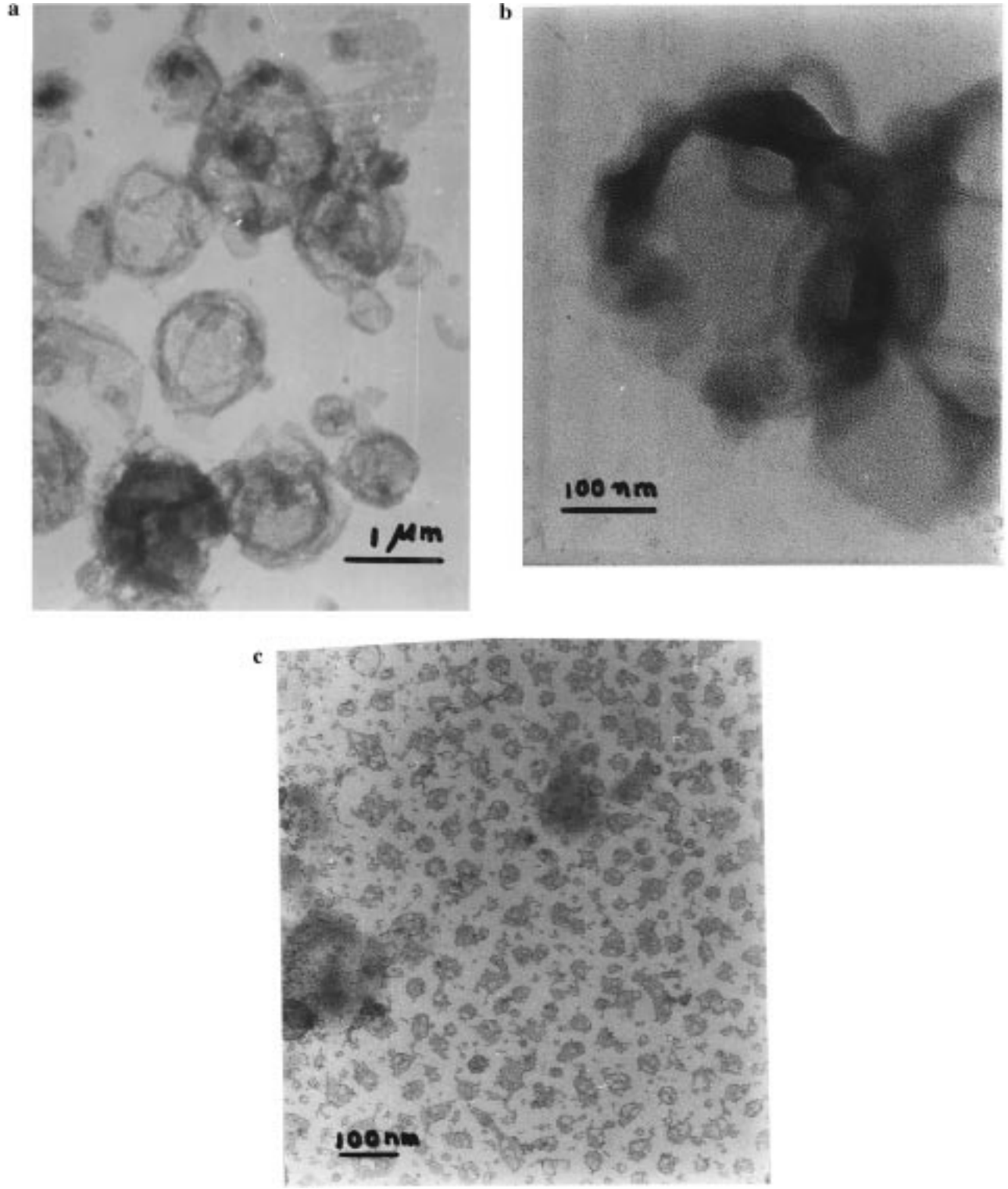


**Figure 1.** (a) Transmission electron micrographs (TEM) of negatively stained liposomes of DMPC from solution; (b) TEM at large magnification of a negatively stained collapsing group of liposomes; (c) TEM of negatively stained DMPC-liposomes + 6SDBs in solution.

sample of noninteracting spheres $|g^{(1)}(\tau)| = \exp(-\Gamma\tau)$, where $\Gamma$ is the decay constant:

$$\Gamma = K^2 D$$

$D$ is the particle diffusion constant, related to the particle radius $r$ by means of the Debye−Stokes−Einstein relationship:

$$D = k_B T/6\pi\eta r$$

where $T$ is the absolute temperature, $k_B$ is the Boltzmann constant, and $\eta$ is the viscosity of the suspending liquid.

$K$ is the magnitude of the scattering vector:

$$K = 4\pi n \sin(\vartheta/2)\lambda_0$$

where $n$ is the refractive index of the suspending liquid, $\vartheta$ is the scattering angle, and $\lambda_0$ is the wavelength of the laser in a vacuum.

For polydisperse samples, particles at each size give rise to a different exponential decay. Therefore,

$$|g^{(1)}(\tau)| = \int_0^\infty G(\Gamma) \exp(-\Gamma\tau)\, d\Gamma$$

where $G(\Gamma)\, d\Gamma$ is the intensity scattered by particles with a decay constant between $\Gamma$ and $\Gamma + d\Gamma$.

A Laplace inversion is required to extract the distribution of decay constants [$G(\Gamma)$] from the above equation. The cumulant analysis is based on the series expansion of ln $|g^{(1)}(\tau)|$ as a function of $(\Gamma\tau)^n$. The coefficients of the expansion are termed "cumulants". The first cumulant measures the mean diffusion coefficient, the second cumulant measures the polydispersity, and the third cumulant provides the distribution asymmetry. In this study we have chosen the so-called "nonnegative least squares" (NNLS)[47,48] as the inversion method. The integral equation for autocorrelation function is simplified as $g = \mathbf{K}x$, where $x$ is the distribution of decay constants and $\mathbf{K}$ is a matrix containing the kernel of the transform. In the kernel matrix, the elements $\exp(-\Gamma_{i\tau j})$ are incremented on $\Gamma_i$ across the rows and on $\tau_j$ across the columns. The algorithm finds the distribution of x which minimizes $||\mathbf{K}x - g||$. The procedure is repeated with several (different but equivalent) sets of assumed sizes over the fit range[49] and then averaged to give a regularized solution. The fit range is estimated by the cumulant analysis.

## Results and Discussion

**Analysis of TEM Measurements.** Figure 1 presents three transmission electron (TE) micrographs of the liposome and liposome + dendrimer systems, with details as follows.

Figure 1a shows the TE micrographs of negatively stained liposomes of DMPC from solution. *The spherical shape and the polydispersity of the liposomes in solution were evident from these results. The diameters ranged from about 0.2 to 1.2 μm*. Taking into consideration that both the vacuum and the staining processes may artificially modify the sizes of the liposomes, the measured sizes were in good agreement with those obtained from DLS measurements (see below).

Figure 1b shows the TE micrograph in large magnification of a collapsing group of liposomes. The main interesting feature, quite rare in TE micrographs, is *the detailed structure of the liposome walls constituted by at least four or five phospholipidic layers. So the preparation process of the liposomes produced mainly multilamellar structures*. In this case, a probe entering the liposome structure may localize in the internal layers that are poorly affected by the dendrimer interaction. Therefore, for the purpose of studying the liposome−SBD interactions, we selected an "external" probe, such as the nitroxide attached to the dendrimer surface.

Figure 1c shows the TE micrograph of negatively stained DMPC-liposome + 6SDB solution. It is interesting that few liposomes "appeared" in the micrographs of solutions in the presence of the dendrimers, which, conversely, were well distinguished. We suppose that the uranyl ions, used in the staining process, were preferentially adsorbed at the dendrimer surface to be complexed by the surface amino groups. As a result, only a small concentration of uranyl ions was adsorbed at the vesicle surface in the presence of the dendrimers.

The 6SBD macromolecules appeared as spheroids of about 200 Å in diameter. The diameter of 6SBD obtained from size exclusion chromatography is about 70 Å.[7] The apparent larger size may again arise from the staining process. Furthermore, larger spheroids indicated the presence of aggregates of dendrimers. No differences in the micrographs were obtained by adding either labeled dendrimers or protonated dendrimers, rather than unlabeled, unprotonated *n*SBDs, to the liposome solution.

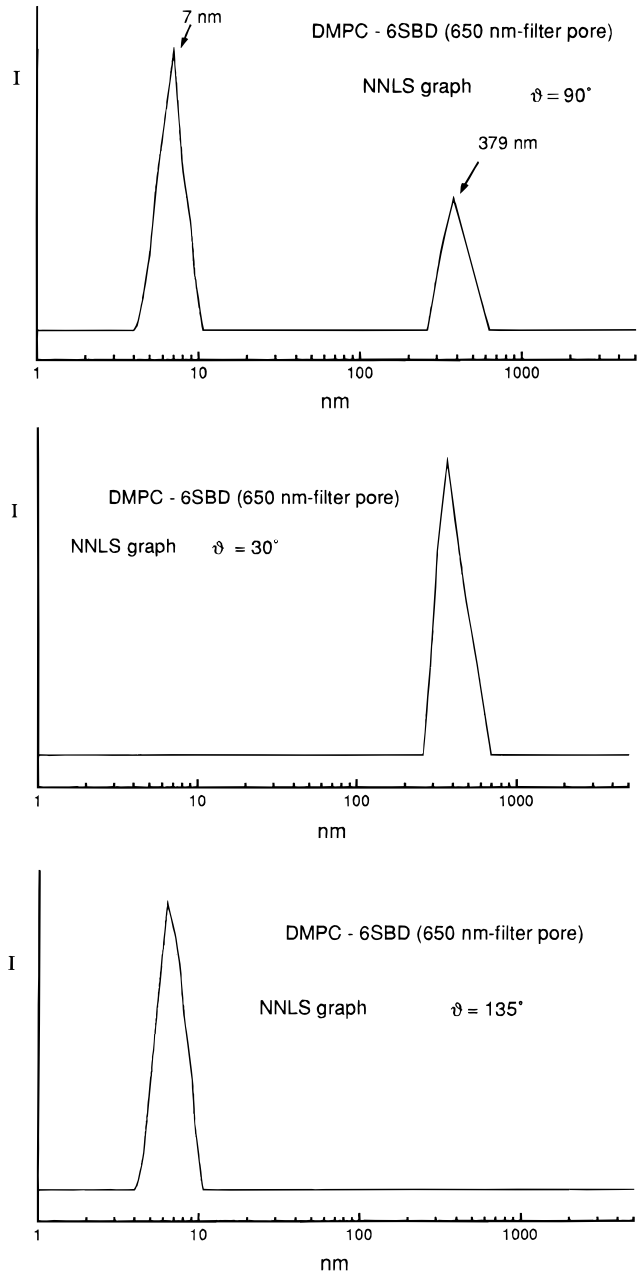


**Figure 2.** NNLS graphs of DMPC-vesicle (indicated as DMPC) + 6SBD solution after double filtration on a 650 nm filter pore, collected at three different diffusion angles: $J = 90°$, 30°, and 135°.

**Analysis of DLS Measurements.** Figure 2 shows the NNLS graphs[45,46] (Theoretical Section, vide supra) of a DMPC-vesicle (indicated as DMPC) + 6SBD solution after double filtration on a 650 nm filter pore and collected at three different diffusion angles: $J = 90°$, 30°, and 135°. Two differently sized populations affected the light scattering. The *larger size particles, with a mean diameter of about 400 nm, were identified as DMPC-vesicles, whereas the smaller size particles, with a mean diameter of about 7 nm, were the dendrimers*. Labeled or protonated dendrimers poorly affected this mean value. Both populations were found at $J = 90°$. The graphs at $J = 30°$ and 135° reproduced the same results as were found for samples of pure liposomes or pure dendrimers, respectively. In fact, the

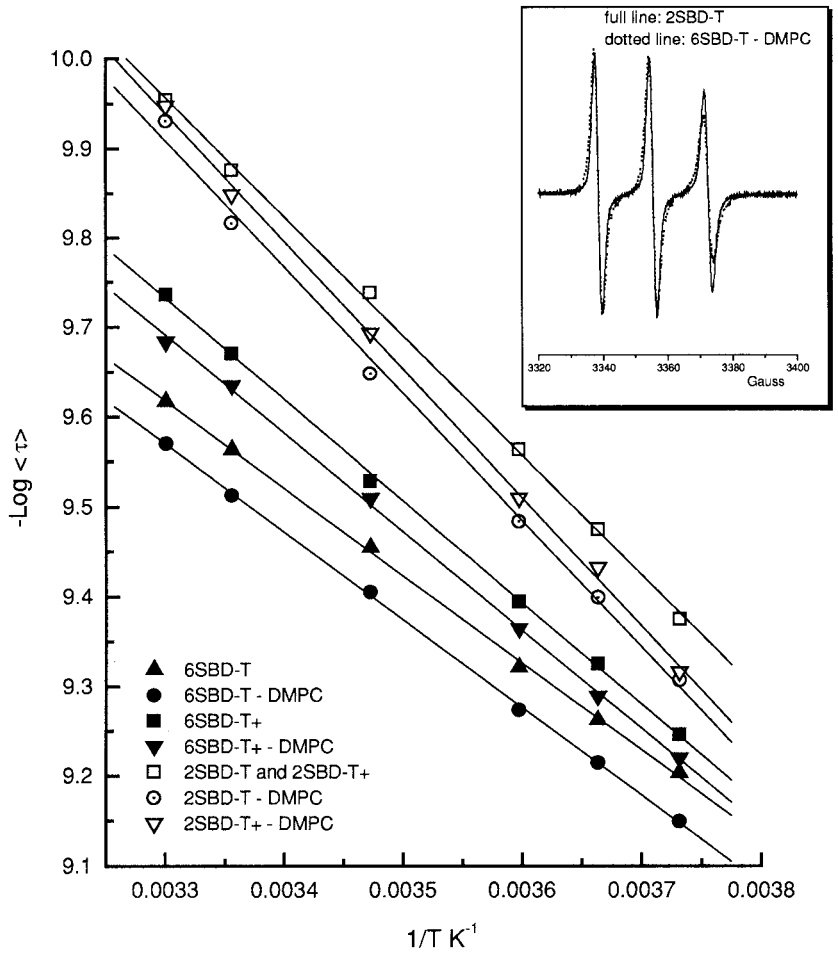


**Figure 3.** Variation of log $\langle\tau\rangle$ as a function of $1/T$ (Arrhenius plot) for the various samples. The inset shows, as examples, the spectrum of 2SBD-T in a water solution (full line) and the spectrum of the 6SBD-T + DMPC-vesicle system (dashed line).

small diffusion angle is evidence of a larger population of particles, whereas the large diffusion angle only allows for LS consisting of small particles.

The graph peaks indicate that the two species, dendrimers and liposomes, do not form any stable assembly and contribute as a supramolecular structure with a differently sized population. On the other hand, the aggregation of one or very few dendrimers with a vesicle cannot be excluded on the basis of the results in Figure 2, since it should not change the mean diameter of the vesicle population: [dendrimer size $\ll$ vesicle size; therefore, (few dendrimers + vesicle)size $\sim$ vesicle size].

**Analysis of EPR Spectra.** EPR spectra taken at room temperature (303 K) of the solutions of the labeled dendrimers, both in the absence and in the presence of the liposomes, consisted of three narrow hyperfine lines, usually found for nitroxide probes under fast motion conditions, characterized by a correlation time for motion $\langle\tau\rangle < (1-2) \times 10^{-9}$ s.[23,33] For example, the inset in Figure 3 shows the spectrum of 2SBD-T in water solution (full line), for which $\langle\tau\rangle = 1.1 \times 10^{-10}$ s, and the spectrum of the 6SBD-T + DMPC-vesicle system (dashed line), for which $\langle\tau\rangle = 2.7 \times 10^{-10}$ s. These two spectra represent the extremes in the variation of the EPR line shape found for the systems under study at room temperature. Table 1 reports correlation times for motion for the label in the various samples at 303 K.

The increase in generation from 2SBD-T to 6SBD-T gave rise to a small decrease in mobility, due to increased packing of the SBD surface groups,[8] whereas both the protonation of the dendrimers and, more significantly, addition of the vesicles provided almost negligible variations in mobility.

**TABLE 1: Correlation Times (303 K) and Activation Energies for Rotational Motion Evaluated from the EPR Spectra**

| system | $\langle\tau\rangle^a(\times 10^{-10}$ s) | $E_a{}^a$ (kcal/mol) |
|---|---|---|
| 2SBD-T | 1.1 | 6.1 |
| 2SBD-T−DMPC | 1.2 | 6.5 |
| 2SBD-T$^+$ | 1.1 | 6.1 |
| 2SBD-T −DMPC | 1.1 | 6.5 |
| 6SBD-T | 2.4 | 4.6 |
| 6SBD-T−DMPC | 2.7 | 4.5 |
| 6SBD-T$^+$ | 1.8 | 5.2 |
| 6SBD-T$^+$−DMPC | 2.0 | 5.1 |

[a] Accuracy $\langle\tau\rangle$ and $E_a$: 2%.

Analysis of the spectra by decreasing the temperature to 268 K showed that the systems obeyed Arrhenius law. At temperatures below the critical temperature transition of DMPC from the liquid-crystal phase to the gel (or solid) phase (296 K),[1,2] the vesicle structure changes and becomes more rigid and organized. However, it is generally assumed that the area of the phosphatidylcholine headgroups (42 Å$^2$) remains almost unchanged upon transition.[1,2] Therefore we expected and assumed that the interactions between the dendrimers and the external vesicle surface were scarcely affected by the structural modification of the vesicles upon transition. The linear variation of log$\langle t\rangle$ as a function of $1/T$ (Arrhenius plot), as reported in Figure 3, also supported this assumption. The Arrhenius plots of the various systems allowed evaluation of the activation energies for rotational motion, $\Delta E^*$. These values are listed in Table 1. The main variation in $\Delta E^*$ was found in the variation in generation.

A decrease in $\Delta E^*$ with an increase in generation has already been described for nitroxide radicals interacting with *n*SBDs.[20] Restriction of degrees of freedom is due to stronger interactions of the radical moiety with the SBD surface groups at later generations and partial trapping at the surface itself. Again, the effect of adding DMPC-liposomes to the SBD-T solutions was quite negligible.

These results clearly indicate that the dendrimers are not permanently attached to the liposome surface; they distribute at different distances from the vesicle surface. On the basis of the chemical nature of the dendrimer and the vesicle surface, we expect that electrostatic and dipolar interactions occur between the groups from the two surfaces. Furthermore, the label rotates rapidly at room temperature, due to the type of link to the SBD surface, and a dipolar or electrostatic interaction slows down this rotation.

Further decrease in temperature below 268 K led to a phase transition in which a portion of the solution was frozen and the dendrimers and vesicles contained in this portion were separated from the remaining solution. This paramagnetic microcrystalline solid did not produce a detectable EPR signal, but rather gave rise to a significant decrease in the intensity of the EPR signal. The remaining portion of solution underwent a glass transition; that is the correspondent EPR spectrum showed a progressive quenching of mobility with the decrease in temperature ("slow motion" conditions with $(1-2) \times 10^{-9}$ s $< \langle\tau\rangle < 5 \times 10^{-7}$ s). It is noteworthy that at about 210 K all the systems showed an almost complete quenching of mobility, as was found at 77 K, and the spectra were computed (results not shown) as powder spectra under so-called rigid conditions ($\langle\tau\rangle > 5 \times 10^{-7}$ s).

Increasing the temperature from 210 K to a range between 250 and 280 K increased the fluidity progressively, and the dendrimer solutions showed interesting differences in the EPR line shape in the absence and presence of the vesicles. This means that *the portion of the solution that underwent glass transition was modified in the rheological properties of the liquid by the occurrence of interactions among the particles*. *Interactions between the dendrimers and the vesicles became EPR-observable and quantifiable.* The results assume relevance with respect to the dendrimer−liposome interactions if we assume that the extent of these interactions is not modified by the cooling−warming process. Fortunately, at about 285 K the ice−liquid water phase transition completely reproduced the situation found at room temperature. Furthermore, reproducibility of the results and stability of the vesicle structure,[1,2] in the temperature range under study, ensure reliability of the parameters obtained from analysis of the spectra at 258 and 277 K, described and discussed in the following paragraphs.

Figures 4 and 5 depict the EPR spectra of SBD-T samples in the absence and in the presence of DMPC-vesicles, obtained at 258 and 277 K, respectively, by increasing the temperature from the rigid conditions. Figures 4a and 5a show the spectra for the 6SBD-T samples, whereas Figures 4b and 5b reported the spectra for the 2SBD-T samples. The full lines are the experimental spectra; the dashed lines are the computed spectra. The main parameters obtained from computation of the spectra (see Theoretical Section, above) are listed in Tables 2 and 3 for the spectra at 258 and 277 K, respectively.

The main findings from analysis of the parameters in Tables 2−3 are as follows.

(a) When two signals contributed to the EPR spectra (at both 258 and 277 K), one contribution invariably showed (i) $\langle\tau\rangle = 2 \times 10^{-9}$ s, (ii) faster rotation of the labels around a direction between the $y-x$ axis, and (iii) a high $A_{zz}'$ value corresponding

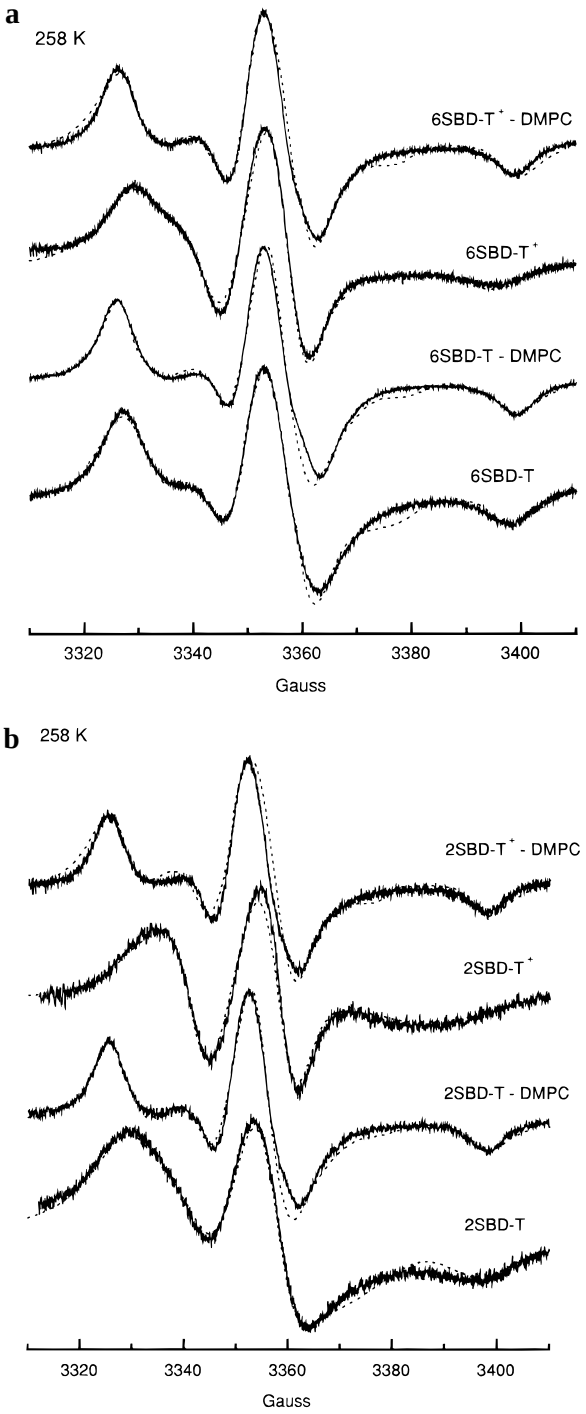


**Figure 4.** EPR spectra of SBD-T solutions in the absence and in the presence of DMPC-vesicles, at 258 K, obtained by increasing the temperature from 210 K. (a) 6SBD-T samples; (b) 2SBD-T samples. Full lines: experimental spectra. Dashed lines: computed spectra.

to the high environmental polarity of the nitroxide group. Upon interactions between the SBD-Ts and the vesicles, the percentage of this contribution decreased with respect to SBD-T without vesicles, in favor of a second contribution indicating (i) slower rotational mobility of the labels, (ii) faster rotation of the labels in a direction between the $z-x$ axis, and (iii) lower environmental polarity of the labels. Therefore *interactions between the dendrimers and the vesicles not only decreased the mobility of the radical moiety but also modified the direction of motion, due to a preferential direction of interaction: probably, the N−O group is initially directed toward the more polar SBD surface and then inserts itself in the less polar hydration layer*

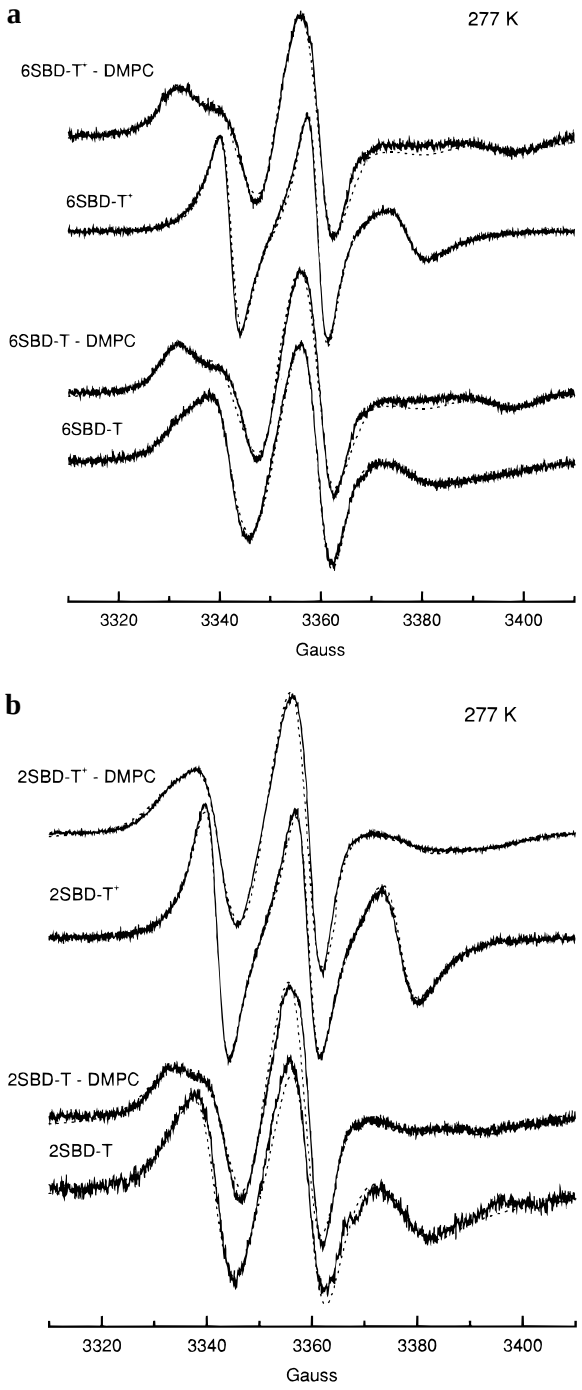


**Figure 5.** EPR spectra of SBD-T solutions in the absence and in the presence of DMPC-vesicles, at 277 K, obtained by increasing the temperature from 210 K. (a) 6SBD-T samples; (b) 2SBD-T samples. Full lines: experimental spectra. Dashed lines: computed spectra.

*at the vesicle surface* (the ESE measurements support this hypothesis, vide infra).

(b) The spectra of the *n*SBD-Ts in the presence of the vesicles at 258 K are quite alike, but all show a significant decrease in rotational mobility of the labels compared to the spectra of the dendrimers without vesicles.

(c) The decrease in mobility from *n*SBD-T systems to *n*SBD-T−DMPC at 258 K was more significant for 2SBD-T than for 6SBD-T and for the protonated dendrimers than for the unprotonated ones; that is, the largest variation of mobility was found for 2SBD-$T^+$, which was still quite mobile at 258 K.

(d) The larger the fluidity of the samples (increasing the temperature to 277 K), the more differentiated were the four

**TABLE 2: Main Parameters for the Computation of the EPR Spectra at 258 K**

| system | $A_{zz}{}^a$ (G) | $\langle\tau\rangle^a$ ($\times 10^{-9}$ s) | main rotation axis - tilt angle | % signal |
|---|---|---|---|---|
| 6SBD-T | 38 | 15.0 | $z-50°$ | 100 |
| 6SBD-T−DMPC | 38 | 23.0 | $z-50°$ | 100 |
| 6SBD-$T^+$ | 39 | 2.3 | $y-50°$ | 30 |
| | 36 | 17.0 | $z-50°$ | 70 |
| 6SBD-$T^+$−DMPC | 38 | 20.0 | $z-50°$ | 100 |
| 2SBD-T | 38 | 8.5 | $z-50°$ | 100 |
| 2SBD-T−DMPC | 38 | 20.0 | $z-50°$ | 100 |
| 2SBD-$T^+$ | 39 | 2.3 | $y-50°$ | 70 |
| | 38 | 4.5 | $z-50°$ | 30 |
| 2SBD-$T^+$−DMPC | 38 | 20.0 | $z-50°$ | 100 |

**TABLE 3: Main Parameters for the Computation of the EPR Spectra at 277 K**

| system | $A_{zz}{}^a$ (G) | $\langle\tau\rangle^a$ ($\times 10^{-9}$ s) | main rotation axis - tilt angle | % signal |
|---|---|---|---|---|
| 6SBD-T | 39 | 2.3 | $y-50°$ | 50 |
| | 36 | 6.0 | $z-50°$ | 50 |
| 6SBD-T−DMPC | 39 | 2.3 | $y-50°$ | 30 |
| | 36 | 15.0 | $z-50°$ | 70 |
| 6SBD-$T^+$ | 39 | 1.5 | $y-50°$ | 100 |
| 6SBD-$T^+$−DMPC | 39 | 2.3 | $y-50°$ | 30 |
| | 36 | 17.0 | $z-50°$ | 70 |
| 2SBD-T | 39 | 2.0 | $y-40°$ | 70 |
| | 36 | 4.0 | $z-50°$ | 30 |
| 2SBD-T−DMPC | 39 | 2.0 | $y-40°$ | 85 |
| | 36 | 6.0 | $z-50°$ | 15 |
| 2SBD-$T^+$ | 39 | 0.9 | $y-50°$ | 100 |
| 2SBD-$T^+$−DMPC | 39 | 2.3 | $y-50°$ | 35 |
| | 36 | 6.0 | $z-50°$ | 65 |

[a] Accuracy: $A_{ii}$ and $\langle\tau\rangle$: 2%.

SBD-T−vesicle samples from each other: (i) *the larger the generation, the lower the mobility (more effective dendrimer−vesicle interactions)*; (ii) *protonated dendrimers showed a larger variation in mobility by adding DMPC (again, more effective dendrimer−vesicle interactions), compared to unprotonated samples*.

**Analysis of ESE Spectra.** Figure 6 shows the 2p-ESE spectrum of 6SBD-T solution (a); the 3p-ESE spectra of 6SBD-T and 6SBD-$T^+$ solutions in the presence of DMPC-vesicles (b); the 2p-ESE spectra of 6SBD-T (c); and 6SBD-$T^+$ (d) solutions in the presence of DMPC-vesicles. All the spectra were recorded in $D_2O$ solutions with [6SBD-T] = 0.05 M and at 4 K. The experimental spectra are the heavier lines, whereas the computed spectra are the thin lines. The parameters used for computation of the modulation and the decay patterns are reported in Table 4. The same parameters were used for the computation of the 2p-ESE and the 3p-ESE signals of the same sample. The spectra of 2SBD-T samples were not reported, since they were almost equivalent to the spectra of the 6SBD-T samples. Both the 3p-ESE spectrum of 6SBD-T and the ESE spectra of 6SBD-$T^+$ solutions (without vesicles) were too noisy and poorly resolved to provide information on the systems and are not reported.

From analysis of the parameters in Table 4, one can see some correspondences and some substantial differences among the samples.

(1) Two shells of deuterium nuclei and one shell of proton nuclei were required for computing the spectra of the three different samples.

(2) One deuterium nucleus constituted the first shell for the three samples. The fitting needed the introduction of a nonzero isotropic hyperfine coupling. This feature meant that *a "complex" is formed between the solvent and the nitroxide radical*.[50]

**TABLE 4: Parameters for the Computation of the Modulation and Decay Patterns of the ESE Signals (ESEEM)**

| system | $n^0D$ | $r_1$[a] (nm) | $a_1$[b] (MHz) | $Q$ (MHz) | $n^0D$ | $r_1$[a] (nm) | $a_1$[b] (MHz) | $Q$ (MHz) | $n^0H$ | $r_1$[a] (nm) | $a_1$[b] (MHz) | $\tau_c$[c] ($\infty$ S |
|---|---|---|---|---|---|---|---|---|---|---|---|---|
| 6SBD-T | 1 | 0.27 | 0.2 | 0.4 | 1 | 0.37 | 0.0 | 0.0 | 2 | 0.27 | −0.1 | 1.0 |
| 6SBD-T−DMPC | 1 | 0.24 | 0.3 | 0.4 | 2 | 0.34 | 0.0 | 0.1 | 4 | 0.30 | 0.0 | 0.3 |
| 6SBD-T$^+$−DMPC | 1 | 0.26 | 0.3 | 0.4 | 2 | 0.34 | 0.0 | 0.1 | 6 | 0.30 | 0.0 | 0.5 |

[a] Accuracy $r_i$ :±0.005 nm. [b] Accuracy $a_i$ and $Q$: ±0.02 MHz. [c] Accuracy $\tau_c$: 10%.

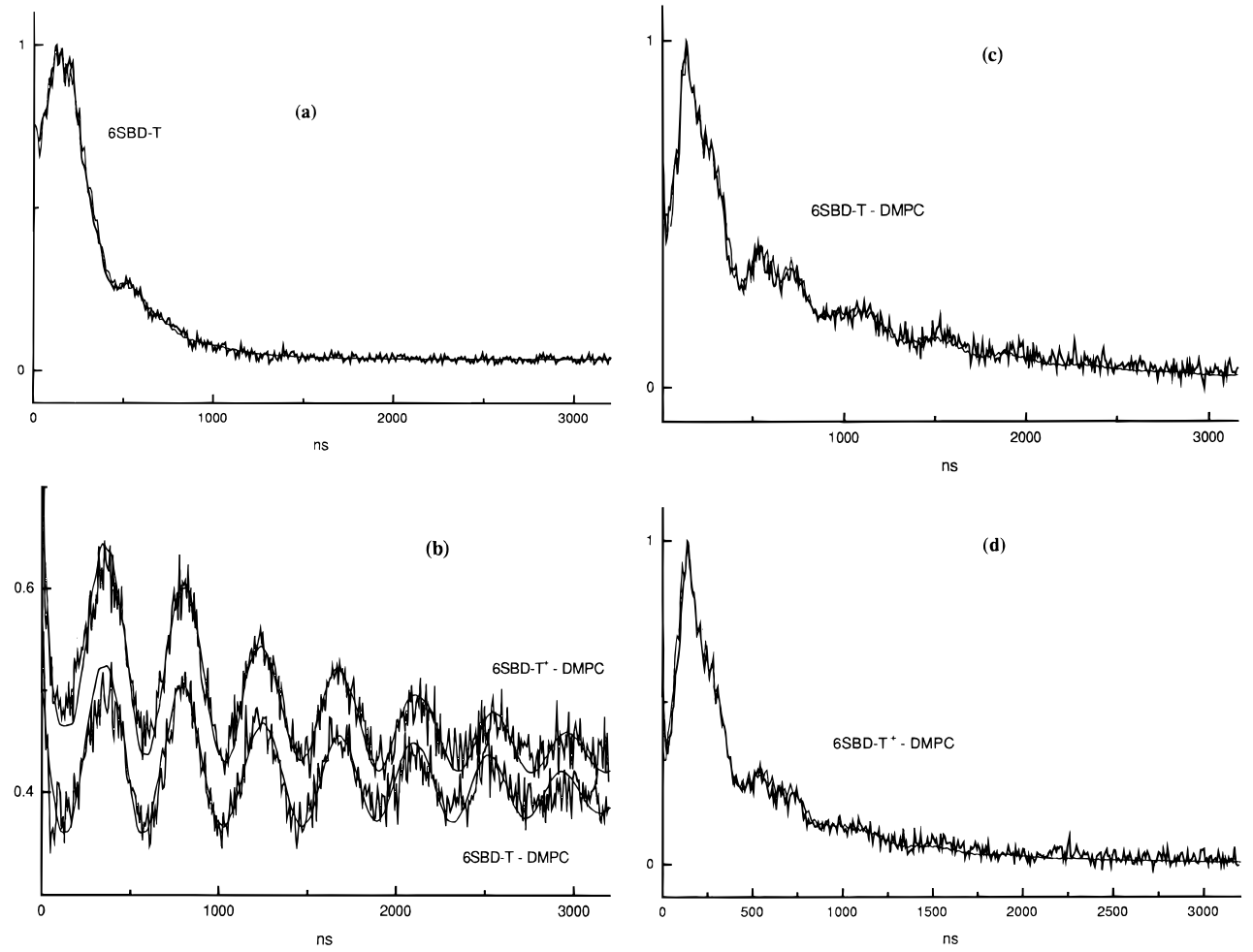


**Figure 6.** (a) 2p-ESE spectrum of 6SBD-T solution; (b) 3p-ESE spectra of 6SBD-T and 6SBD-T$^+$ solutions in the presence of DMPC-vesicles; (c) 2p-ESE spectrum of 6SBD-T−DMPC-vesicles; (d) 2p-ESE and 6SBD-T$^+$−DMPC-vesicles. Spectra recorded in $D_2O$ solutions, with [6SBD-T] = 0.05 M, and at 4 K. Experimental spectra: thick lines. Computed spectra; thin lines.

One O−D group belonging to the solvent approached the N−O moiety at a distance between 0.24 and 0.27 nm.

(3) The distance of the unpaired electron from the "complexed" $D_2O$ was slightly shorter for the 6SBD-T−DMPC-vesicle sample than for the other two samples.

(4) More significantly, the number of deuterium nuclei increased from the 6SBD-T solution without vesicles (one deuterium) to the 6SBD-T samples in the presence of the vesicles (two deuteria). The findings for points (3) and (4) have the same explanation; that is, *the interaction of the SBD-T with the vesicle partially compressed the hydration layer of the N−O group, and/or the hydration layer of the vesicle headgroups approached the unpaired-electron site*.

(5) Two protons are coupled with the unpaired electron for the 6SBD-T sample. The distance between the protons of the methylene group of the doxyl ring and the N−O group is 0.35 nm,[35] which is farther than the distance we evaluated from computation (0.27 nm). Probably, the coupled protons belonged to the SBD surface, indicating that *the bonds linking the nitroxide group to the SBD surface are bent in order to allow the N−O group to approach the surface itself*. This is in line with the fast-rotation of the radical around a direction between the $y-x$ axes, as found from CW-EPR analysis.

(6) The number of electron-coupled protons increased from 6SBD-T to 6SBD-T − DMPC (4 protons, 0.30 nm) and to 6SBD-T$^+$−DMPC (6 protons). This result may be considered a consequence of the shift in the main rotation axis from $y-x$ intermediate direction to $z-x$ intermediate direction (from CW-EPR analysis): *due to dendrimer−vesicle interaction, the N−O group oriented itself toward the SBD surface, and consequently, it increased the number of SBD protons coupled with the unpaired electron.*

(7) The different orientation of the nitroxide group to promote its interaction with the vesicle surface was also responsible for the increased freedom of motion of the methyl groups, whose rotation was faster for 6SBD-T−DMPC ($\tau_c$ = 0.3 $\mu$s) and 6SBD-T$^+$−DMPC ($\tau_c$ = 0.5 ms) than for 6SBD-T samples ($\tau_c$ = 1.0 ms).

## Conclusion

Transmission electron micrographs of negatively stained DMPC-liposomes, both in the absence and in the presence of *n*SBDs, showed the spherical shape and the polydispersity of liposomes in solution. The diameters ranged from about 0.2 to 1.2 mm. The staining process was responsible for the "disappearance" of the vesicles in the presence of the dendrimers and of the larger size of the 6SBDs (diameter ∼200 Å) compared to the values obtained from size exclusion chromatography (diameter ∼70 Å). Magnified micrographs showed that the liposome walls consisted of at least four or five phospholipidic layers (multilamellar structures), which promoted the use of an external label (labeled dendrimers) for the EPR measurements.

Analysis of the DLS results of filtered (650 nm pore filter) solutions provided the mean vesicle diameter of about 400 nm, whereas the 6SBD diameter was 7 nm. Mean size did not change when both dendrimers and vesicles were present in solution, an indication that permanent supramolecular dendrimer−vesicle structures were not formed. EPR measurements at room temperature also indicated that the *n*SBDs distributed in the solution regions at different distances between the vesicle surface and the *n*SBD surface. Mainly dipolar and electrostatic interactions occurred between dendrimer and liposome surface groups, which inefficiently slowed the fast rotation of the labels.

Interactions between dendrimers and vesicles (tested by a decrease in rotational mobility of the label) become EPR-observable and quantifiable by (i) eliminating the fraction of dendrimers not affected by the interactions with the vesicles (below the freezing transition of a portion of the solution) and (ii) retaining fluidity (in the range 250−280 K) of a fraction of the dendrimers affected by interactions with the vesicles.

The main conclusions that are quantitatively demonstrated by changes in the parameters obtained from CW-EPR and ESEEM analyses are as follows.

(1) Dendrimer−vesicle interactions modify the direction of the fast-rotation axis of the radical.

(2) Dendrimer−vesicle interactions are stronger for (i) later generations than for earlier generations and (ii) protonated SBD-T surfaces than for unprotonated ones.

(3) A "complex" is formed between a single solvent molecule and the nitroxide radical.

(4) Interaction between the SBD-T surface and the vesicle partially compressed the hydration layer of the N−O group; and/or the hydration layer of the vesicle headgroups is compressed onto the unpaired-electron site.

This study provides useful information on the role that starburst dendrimers play as gene carriers: (i) the dendrimers interacted with the membrane surface, but did not permanently perturb the membrane properties (enhanced biocompatibility); (ii) measurements at low temperatures indicated that interaction is more effective for protonated dendrimers at larger sizes (later generations), which, therefore, have more potential as carriers of biomolecules to approach the cell membrane.

Studies of dendrimer−vesicle interactions in the presence of biomolecules, such as DNA and polynucleotides, are in progress.

**Acknowledgment.** The authors thank Dr. Patrizia Maccone for help in performing and analyzing the DLS measurements, Dr. Massimo Bigazzi for help in performing and analyzing the TEM measurements, and Prof. M. Romanelli for providing the programs used in computing the ESE patterns. N.J.T. thanks the National Science Foundation and NATO for their generous support. D.A.T. thanks the New Energy and Development Organization (NEDO) of the Ministry of International Trade and Industry of Japan (MITI) for its generous support and certain critical synthetic efforts. M.F.O. and P.M. thank the Italian Ministero Università e Ricerca Scientifica e Tecnologica (MURST) for its financial support.

## References and Notes

(1) *Vesicles*; Surfactant Science Series; Rosoff, M., Ed.; M. Dekker: New York, 1996; Vol. 62.

(2) (a) Lasic, D. D. *Liposomes: From Physics to Applications*; Elsevier: Amsterdam, 1993; (b) *Liposomes*; Knight, C. G., Ed.; Elsevier: Amsterdam, 1981. (c) *Liposomes. A Practical Approach*; New, R. R. C., Ed.; Oxford University Press: Oxford, 1990.

(3) Fendler, J. H. *Membrane Mimetic Chemistry*; Wiley-Interscience: New York, 1982.

(4) Strom-Jensen, P. R.; Magin, R. L.; Dunn, F. *Biochim. Biophys. Acta* **1984**, *769*, 179.

(5) Maynard, V. M.; Magin, R. L.; Dunn, F. *Chem. Phys. Lipids* **1985**, *37*, 1.

(6) (a) *Advances in Dendritic Macromolecules*; Newkome, G. R., Ed.; JAI Press: Greenwich, CT, 1993. (b) Newkome, G. R.; Moorefield, C. N.; Baker, G. R.; Johnson, A. L.; Behera, R. K. *Angew. Chem., Int. Ed. Engl.* **1991**, *30*, 1176. (c) Makelburger, H. B.; Jaworek, W.; Vögtle, F. *Angew. Chem., Int. Ed. Engl.* **1992**, *31*, 1571. (d) Issberner, J.; Moors, R.; Vögtle, F. *Angew. Chem., Int. Ed. Engl.* **1994**, *33*, 2413. (e) Alper, J. *Science* **1991**, *251*, 1562. (f) Krohn, K. *Org. Synth. Highlights* **1991,** 378. (g) Amato, L. *Sci. News* **1990**, *138*, 298. (h) Kim, Y. H.; Webster, O. W. *J. Am. Chem. Soc.* **1990**, *112*, 2, 4592. (i) Hawker, C. J.; Wooley, K. L.; Fréchet, J. M. J. *J. Chem. Soc., Perkin Trans. 1* **1993**, 1287. (j) Fréchet, J. M. J. *Science* **1994**, *263*, 1710.

(7) (a) Tomalia, D. A.; Hall, M.; Hedstrand, D. M. *J. Am. Chem. Soc.* **1987**, *109*, 1601. (b) Tomalia, D. A.; Naylor, A. M.; Goddard, W. A., III. *Angew Chem. Int. Ed. Engl.* **1990**, *29*, 138. (c) Tomalia, D. A.; Durst, H. D. In *Topics in Current Chemistry*; Weber, E., Ed.; Springer-Verlag: Berlin, Heidelberg, 1993; Vol. 165, p 193.

(8) Naylor, A. M.; Goddard, W. A., III; Kiefer, G. E.; Tomalia, D. A. *J. Am. Chem. Soc.* **1989**, *111*, 2341.

(9) Tomalia, D. A. *Adv. Mater.* **1994**, *6*, 7.

(10) Jansen, J. F. G. A.; deBrabander, E. M. M.; Meijer, E. W. *Science* **1994**, *266*, 1226.

(11) Mattei, S.; Seiler, P.; Diederich, F. *Helv. Chim. Acta* **1995**, *78*, 1904.

(12) Turro, C.; Niu, S.; Bossmann, S. H.; Tomalia, D. A.; Turro, N. J. *J. Phys. Chem.* **1995,** *99*, 5512.

(13) For recent literature see the following selections and references therein: (a) Schurtenberger, P.; Hauser, H. In *Liposome Technology*, 2nd ed.; Gregoriadis, G., Ed.; CRC Press, Inc.: Boca Raton, FL, 1993; p 253. (b) Hallett, F. R.; Watton, J.; Krygsman, P. *Biophys. J.* **1991**, *59*, 357. (c) Van Zanten J. H.; Monbouquette, H. G. *J. Colloid Interface Sci.* **1991**, *146*, 330. (d) *Ibid.* **1994**, *165*, 512.

(14) Zhao, G.-X., Yu, W.-L. *J. Colloid Interface Sci.* **1995**, *173*, 159.

(15) Bonaccio, S.; Wessicken, M.; Berti, D.; Walde, P.; Luisi, P. L. *Langmuir* **1996**, *12*, 4976.

(16) Marsh, D.; Watts, A. In *Liposomes;* Knight, C. G., Ed.; Elsevier: Amsterdam, 1981; p 139.

(17) Lasic, D. D. *Bull. Magn. Reson.* **1991**, *13*, 3. Lasic, D. D. *J. Phys.* **1983**, *44*, 737.

(18) Lomax, T. L.; Mehlhorn, R. J. *Biochim. Biophys. Acta* **1985,** 106.

(19) (a) Korstanje, L. J.; van Fassen, E. E.; Levine, Y. K. *Biochim. Biophys. Acta* **1989**, *882*, 196. (b) de Jongh, H. H. J.; Hemminga, M. A.; Marsh, D. *Biochim. Biophys. Acta* **1990**, *1024*, 82. (c) Datema, K. P.; Wolfs, C. J. A. M.; Marsh, D.; Watts, A.; Hemminga, M. A. *Biochemistry* **1987**, *26*, 7571.

(20) Ottaviani, M. F.; Cossu, E.; Turro, N. J.; Tomalia, D. A. *J. Am. Chem. Soc.* **1995** *117*, 4387.

(21) (a) Ottaviani, M. F.; Turro, N. J.; Jockusch, S.; Tomalia, D. A. *J. Phys. Chem.* **1996**, *100*, 13675. (b) Ottaviani, M. F., Turro, N. J.; Jockusch, S.; Tomalia, D. A. *Colloids Surf.* **1996**, *115*, 9.

(22) Ottaviani, M. F.; Andechaga, P.; Turro, N. J.; Tomalia, D. A. *J. Phys. Chem. B* **1997**, *101*, 6057.

(23) (a) *Spin Labeling. Theory and Applications*; Berliner, L. J., Ed.; Academic Press: New York, 1976; Vol. 1; 1979; Vol. 2. (b) *Biological Magnetic Resonance. Spin Labeling. Theory and Applications*; Berliner, L. J.; Reuben, J., Eds.; Plenum Press: New York, 1989; Vol. 8.

(24) (a) *Modern Pulsed and Continuous-Wave Electron Spin Resonance*; Kevan L., Bowman, M. K., Eds.; Wiley-Interscience: New York, 1990. (b) *Time Domain Electron Spin Resonance*; Kevan, L., Schwartz, R., Eds.; Wiley-Interscience: New York, 1979.

(25) (a) Hiromitsu, I.; Kevan, L. *J. Am. Chem. Soc.* **1987**, *109*, 4501. (b) Hiff, T.; Kevan, L. *J. Phys. Chem.* **1989**, *93*, 1572.

(26) Ottaviani, M. F.; Daddi, R.; Brustolon, M.; Turro, N. J.; Tomalia, D. A. *Appl. Magn. Reson.* **1997**, *13*, 347.

(27) Reeves, J. P.; Dowben, R. M. *J. Cell. Physiol.* **1969,** *73*, 49.
(28) Dvornic, P. R.: Tomalia, D. A. *Macromol. Symp.* **1994**, *88*, 123.
(29) Pauly, G. T.; Bobst, E. V.; Bruckmann, D.; Bobst, A. M. *Helv. Chim. Acta* **1989**, *72*, 110.
(30) Ottaviani, M. F.; Montalti, F.; Turro, N. J.; Tomalia, D. A. *J. Phys. Chem.* **1996**, *100*, 11033.
(31) (a) Hashimoto, S.; Thomas, J. K. *J. Am. Chem. Soc.* **1983**, *105*, 5230. (b) Baglioni, P.; Kevan, L. *J. Phys. Chem.* **1987**, *91*, 1516.
(32) Kunitake, T.; Okahata, U. *J. Am. Chem. Soc.* **1980**, *102*, 549.
(33) Schneider, D. J., Freed, J. H. In *Biological Magnetic Resonance. Spin Labeling. Theory and Applications*; Berliner, L. J., Reuben, J., Eds.; Plenum Press: New York, 1989; Vol. 8, p 1.
(34) Dzuba, S. A.; Maryasov, A. G.; Salikhov, K. M.; Tsvetkov, Yu. D. *J. Magn. Reson.* **1984**, *58*, 95.
(35) Dikanov, S. A.; Shubin, A. A.; Parmon, V. N. *J. Magn. Reson.* **1981**, *42*, 474.
(36) Schweiger, A. *Angew. Chem.* **1991**, *30*, 265.
(37) Atherton, N. M. *Principles of Electron Spin Resonance*; Ellis Horwood and Prentice Hall: New York, 1993.
(38) Schweiger, A. In *Modern Pulsed and Continuous-Wave Electron Spin Resonance*; Kevan, L., Bowman, M. K., Eds.; Wiley: New York, 1990.
(39) (a) Kevan, L. In *Time Domain Electron Spin Resonance*; Kevan, L., Schwartz, R., Eds.; Wiley-Interscience: New York, 1979; Chapter 8. (b) Salikhov, K. M.; Tsvetkov, Yu. D. In *Time Domain Electron Spin Resonance*; Kevan, L., Schwartz, R., Eds.; Wiley-Interscience: New York, 1979; Chapter 7. (c) Brown, I. M. In *Time Domain Electron Spin Resonance*; Kevan, L., Schwartz, R., Eds.; Wiley-Interscience: New York 1979; Chapter 6. (d) Mims, W. B. *Phys. Rev.* **1968**, *168*, 370.
(40) Romanelli, M.; Kevan, L. *J. Magn. Reson*. **1991**, *91*, 549.
(41) Heming, M.; Narayana, M.; Kevan, L. *J. Chem. Phys.* **1985**, *83*, 1478.
(42) Mims, W. B. *Phys. Rev. B* **1972**, *5*, 2409.
(43) Allen, P. S.; Cowking, A. *J. Chem. Phys*. **1968**, *49*, 789.
(44) (a) Bott, S.E. in *Particle Size Analysis*; Lloyd, P. J., Ed.; Wiley: London, 1988; p 77. (b) Cummins, P. G.; Staples, E. J. *Langmuir* **1987**, *3*, 1109. (c) Finsy, R.; De Groen, P.; Deriemaeker, L. Geladé, E.; Joosten, J. *Part. Part. Syst. Charact.* **1992**, *9*, 237. (d) Wu, C.; Unterforsthuber, K.; Lilge, D.; Luddecke, E.; Horn, D. *Part. Part. Syst. Charact.* **1994**, *11*, 145.
(45) (a) Bryant, G.; Thomas, J. C. *Langmuir* **1995**, *11*, 2480. (b) Bryant, G.; Abeynayake, C.; Thomas, J. C. *Langmuir* **1996**, *12*, 6224.
(46) (a) Chu, B. *Laser Light Scattering*, 2nd ed.; Academic Press: New York, 1991. (b) Brown, W., Ed. *Dynamic Light Scattering: The Method and Some Applications*; Claredon Press: Oxford, 1993. (c) Finsy, R. *Adv. Colloid Interface Sci.* **1994**, *52*, 79.
(47) Lawson, C. L.; Hanson, R. J. *Solving Least Squares Problems*; Prentice Hall: Englewood Cliffs, NJ, 1974.
(48) (a) Grabowski, E. F.; Morrison, I. D. in *Measurement of Suspended Particles by Quasi-Elastic Light Scattering*; Dahneke, B. E., Ed.; Wiley-Interscience: New York, 1986; p 199. (b) Morrison, I. D.; Grabowski, E. F.; Herb, C. A. *Langmuir* **1985**, *4*, 496.
(49) McWhirter, J. G.; Pike, E. R. *J. Phys. A Math. Gen.* **1978**, *11*, 1729.
(50) (a) Romanelli, M.; Martini, G.; Kevan, L. *J. Phys. Chem.* **1988**, *92*, 1958. (b) Romanelli, M.; Ottaviani, M. F.; Martini, G.; Kevan, L. *J. Phys. Chem.* **1989**, *93*, 317.